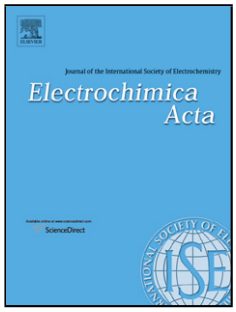

Title: Formation and characterization of Fe^{3+}-/Cu^{2+}- modified zirconium oxide conversion layers on zinc alloy coated steel sheets

Author: Thomas Lostak Stefan Krebs Artjom Maljusch Till Gothe Miroslaw Giza Matthias Kimpel Jörg Flock Stephan Schulz

PII: S0013-4686(13)01691-5
DOI: http://dx.doi.org/doi:10.1016/j.electacta.2013.08.161
Reference: EA 21186

To appear in: *Electrochimica Acta*

Received date: 20-6-2013
Revised date: 26-8-2013
Accepted date: 26-8-2013

Please cite this article as: T. Lostak, S. Krebs, A. Maljusch, T. Gothe, M. Giza, M. Kimpel, J. Flock, S. Schulz, Formation and characterization of Fe^{3+}-/Cu^{2+}- modified zirconium oxide conversion layers on zinc alloy coated steel sheets, *Electrochimica Acta* (2013), http://dx.doi.org/10.1016/j.electacta.2013.08.161

Formation and characterization of Fe^{3+}- / Cu^{2+}-modified zirconium oxide conversion layers on zinc alloy coated steel sheets

Thomas Lostak,[‡*] Stefan Krebs,[‡] Artjom Maljusch,[§] Till Gothe,[‡] Miroslaw Giza,[‡] Matthias Kimpel,[‡] Jörg Flock,[‡] Stephan Schulz[†]

[‡] *ThyssenKrupp Steel Europe AG, Research and Development, Kaiser-Wilhelm-Straße 100, 47166 Duisburg, Germany*

[†] *Universität Duisburg-Essen, Faculty of Chemistry, Universitätsstraße 7, 45141 Essen, Germany*

[§] *Ruhr-Universität Bochum, Analytische Chemie – Elektroanalytik & Sensorik, Universitätsstraße 150, 44780 Bochum, Germany*

Abstract

Zirconium oxide conversion layers are considered as environmentally friendly alternatives replacing chromate-based passivation layers in the coil-coating industry. Based on excellent electronic barrier properties they provide an effective corrosion protection of the metallic substrate. In this work, thin layers were grown on HDG-steel-substrates by increasing the local pH at the surface and were characterized using potentiodynamic polarization technique. The influence of $Cu(NO_3)_2{\cdot}3H_2O$ or $Fe(NO_3)_3{\cdot}9H_2O$ on morphology and thickness of deposited protective layers were investigated by XPS, ToF-SIMS and FE-SEM. A significant film thickness increase was found by adding Cu^{2+} or Fe^{3+} ions to the conversion solution. In addition, growth kinetics were studied by *in-situ* measurements of corrosion potential using potentiodynamic polarization technique.

[*]Corresponding author
Email address: thomas.lostak@thyssenkrupp.com
Phone: +49 203 52-244657
Fax: +49 203 52-228723

Keywords: ZrO_2, zinc alloy coated steel sheets, conversion layer, corrosion potential, corrosion protection,

1. Introduction

Pretreatment systems for organic coatings are commonly applied to metal surfaces to improve their adhesion properties and corrosion resistance. In the near future, classical industrial pretreatment systems such as chromate passivation or trication phosphatation have to be replaced due to their harmful properties and ecological disadvantages [1]. Recently, new environmentally friendly pretreatment technologies have been developed. The most interesting candidates for these sophisticated surface coatings are organosilanes [2–6], lighter rare earth metals [7,8] and transitional metals [9], respectively. Moreover, promising alternatives are the application of zirconium containing layers on the metal surface by the sol-gel process [10–13] or by immersion in hexafluorozirconic acid (H_2ZrF_6) conversion solution [14–24].

Formation mechanism, film morphology as well as composition of zirconium oxide layers have been studied in detail on aluminium alloys [14–16]. It was shown that the film formation mechanism largely depends on the alloy composition, which mainly determines the electrochemical behaviour of the metallic substrates [19,25]. Andreatta et al. [19] examined different stages of film formation process using a scanning Kelvin probe force microscopy (SKPFM). In their publication, authors showed that the deposition of the conversion layer is an electrochemically driven process and starts on the α-Al(Fe,Mn)Si intermetallic particles present in the aluminium alloy due to specific cathodic reactions like hydrogen evolution and oxygen reduction. Subsequently, the zirconium oxide layer indicates lateral growth around these regions and covered with longer immersion times the entire surface of the metallic substrate. The improved corrosion protection offered by this coating was studied using potentiodynamic polarization and corrosion potential measurements both performed in NaCl electrolyte. George et al. [25] investigated the influence of copper addition to aluminium on

the formation of zirconium-based conversion layer using different surface analytical methods (SEM, TEM, Rutherford backscattering spectroscopy (RBS), nuclear reaction analysis (NRA) and glow discharge optical emission spectroscopy (GDOES)). It was shown that the addition of copper to aluminium results in a slowing of the rate of layer formation, particularly for Cu content above 5 at.%. The oxidation rate of the substrate was barely not affected by the addition of copper. Authors proposed that the copper species impede the transport of cationic species to the coating base. Beyond that, copper promotes the formation of a layer of corrosion products beneath the conversion coating, which could influence the deposition process [25].

Here, hot-dip galvanized steel (HDG) was chosen as a substrate since this material is of major interest for a number of technological applications, in particular in the automobile industry [26]. Surprisingly, despite the high technological importance of this substrate material, the number of reports in this area is significantly smaller compared to those using other metallic substrates such as magnesium [22,27] or aluminium alloys [14,17]. Several groups investigated environmentally friendly conversion layers by means of different surface analytical and electrochemical methods using commercial solutions, with more or less unknown chemical composition [20,21,23,24,28,29]. Adhikari et al. [24] characterized coatings formed by copper containing conversion solutions on different metallic substrates, using AFM, Scanning transmission electron microscopy (STEM), X-Ray energy dispersive spectroscopy (XEDS) and complementary electrochemical techniques. It was found that the copper containing conversion solution lead to thicker conversion coatings at same immersion times. Coatings were primarily composed of Zr, O and Fe, while enrichments of F were detected close to the coating-steel interface. The Cu deposits were randomly distributed within the coating. This study clearly shows that chemical acceleration of this new kind of environmentally friendly pretreatment is possible [24].

Because there is still a lack in knowledge about the film formation processes in environmentally friendly conversion solutions, in this study the film formation process on hot-dip galvanized steel in an aqueous model conversion solution based on hexafluorozirconic acid was investigated. The novel aspects of this work are the characterization and comparison of film formation process in a conversion solution with known composition, on the one hand, and investigation of improvement of the kinetics of growth of the conversion layer in conversion solutions containing different additives, on the other hand. Used additives are $Fe(NO_3)_3 \cdot 9H_2O$ and $Cu(NO_3)_2 \cdot 3H_2O$ while only the latter was reported by Adhikari et al. in combination with a conversion solution of commercial blend with an unknown composition [24].

The conversion layer thickness and composition were determined using X-ray photoelectron spectroscopy (XPS) and the homogeneity of the protective layer was investigated by time-of-flight secondary ion mass spectroscopy (ToF-SIMS). Information about the layer morphology was obtained by scanning electron microscopy (SEM). *In-situ* corrosion potential measurements were performed to study the growth kinetics of the conversion layer. The barrier properties and corrosion protection performance of deposited conversion layers were characterized using potentiodynamic polarization technique.

2. Experimental

2.1 Materials and sample preparation

Samples of line produced non-temper rolled galvanized steel blanks with a diameter of 5 cm (ThyssenKrupp Steel Europe AG) were used. The galvanized layer contains 98.52 % Zn and 1.08 % Al by weight. Prior FE-SEM measurements, the samples were polished with SiC 500 grit paper and then with 1 µm Al_2O_3-oxide polishing suspension. The polishing procedure did not affect the chemical composition of the zinc coated steel sheets. To ensure reproducible clean surfaces, all samples were degreased using an automated cleaning system (WESERO GmbH, Germany). The cleaning procedure contains following steps:

Step 1 - Ridoline® C72 (Henkel KGaA, Germany), 8 g/l, 70 ± 5 °C, pH 11 (cleaning time: 8 s)

Step 2 - Ridoline® 1340 (Henkel KGaA, Germany), 16-20 g/l, 70 ± 5 °C, pH 9.9 (cleaning time: 8 s)

Step 3 - Rinsing with deionized water (50 °C, $\kappa = \leq 4$ µS/cm)

Step 4 - Drying in warm stream of air

2.2 Deposition of conversion layer

The deposition of conversion layer was performed directly after degreasing of substrates. The conversion solution was prepared by adding 0.1 mmol $Cu(NO_3)_2 \cdot 3H_2O$ (HZF+Cu) or $Fe(NO_3)_3 \cdot 9H_2O$ (HZF+Fe) (Merck, Germany) to the hexafluorozirconic acid (H_2ZrF_6) (HZF) solution (1 mmol/l; alufinish GmbH & Co KG, Germany). The pH value of the conversion solution was adjusted to pH 4 using ammonium bicarbonate (NH_4HCO_3, 10 wt.%) as buffer agent. Immersion of samples was performed under solution stirring (300 rpm) at ambient temperature ($T \sim 20$ °C). After finishing the deposition process, all substrates were rinsed with ultrapure water ($T \sim 20$ °C, $\kappa \leq 0{,}005$ µS/cm) and dried in a stream of nitrogen gas.

2.3 Surface analytical techniques

ToF-SIMS

The ToF-SIMS analysis was carried out on a gridless reflectron based ToF-SIMS 5 (iontof GmbH, Germany) equipped with a bismuth-cluster ion source. All spectra and images were obtained using Bi_3^+ primary ions at 25 keV energy in high current bunched mode with a mass resolution of $m/\Delta m$ = 5000 (at mass 55 u, $C_4H_7^+$). The beam diameter was about 3-5 µm and all measurements were made under static conditions (primary ion dose density < F_{PI} = $5x10^{12}$ ions /cm^2) on an area of 400x400 µm with 256x256 pixels resolution.

XPS

The chemical compositions of conversion layers were investigated by a Quantum 2000 ESCA Microprobe (Physical Electronics Inc., USA). All spectra were obtained using a monochromated Al K_α-beam with a spot size of 100x100 µm. The take-off angle of the detected photoelectrons was 45° to the surface normal. The C1s peak (binding energy of 284.8 eV) was used as internal reference for all spectra. The quantification of all elements was performed on the basis of survey spectra. Depth profiling was performed using Ar^+ ion sputtering with an acceleration voltage of 2 kV and sputter rate of 10 nm/min. A silicon wafer containing a well-defined oxide layer of known thickness was used for depth calibration. The fitting of the measured XPS spectra was performed through the CasaXPS software.

FE-SEM

The morphology of coating layers was studied with a high resolution FE-SEM Merlin® microscope (Carl Zeiss Microscopy GmbH, Germany) equipped with an EDX analysis device (EDAX Ametek GmbH, Germany). The microscope was equipped with an inlense detector.

The working distance between the sample and the pole shoe was 2 mm. The primary electron beam acceleration was 1 kV (SE1).

2.4 Electrochemical techniques

The electrochemical measurements were performed using an Autolab potentiostat (Metrohm GmbH & Co. KG, Germany) and a three-electrode arrangement consisting of the working electrode (1 cm² of sample surface was exposed), Ag/AgCl reference electrode with inner filling of 3 mol/L KCl (+0.209 V_{SHE} at ambient temperature) and a platinum mesh as a counter electrode. The counter and working electrode were placed parallel with a distance of 6 cm, the volume of the cell was about 250 ml. Electrochemical measurements of corrosion potential during the formation of conversion layers were performed under analogous deposition conditions as described for the deposition of conversion layer. The polarization curves were recorded from -1.1 V_{SHE} to about -0.4 V_{SHE} with a scan rate of 5 mV/s in oxygen saturated 0.1 M Na_2SO_4 aqueous solution at room temperature. The corrosion current densities were determined according to the method of Allen and Hickling [30]. For statistical reasons each measurement was repeated three times.

3. Results and Discussion

3.1 Surface composition of deposited zirconium-based conversion layers

To investigate the influence of different additives on the film formation kinetics, HDG substrates were immersed in conversion solutions for different times. XPS was applied to obtain detailed information about the chemical composition and film thickness of deposited conversion layers. Table 1 shows the chemical surface composition of samples immersed in conversion solution for 60 s and 300 s, while an untreated HDG sample was used as a reference. The uppermost layer of a non-temper rolled, untreated HDG sample consists of 2-3 nm thick Al-oxyhydroxide layer. After alkaline cleaning 29 at.% of zinc, 60 at.% of oxygen and 11 at.% of aluminum were detected on the sample surface indicating the partly removal of thin Al-oxyhydroxide layer during alkaline etching. This observation correlates well with data previously reported by Fink et al. [31]. Main components of the conversion layer are oxygen and zirconium. Additionally, zirconium oxide layer contains small quantities of metallic zinc (~ 4-8 at.%), most likely originating from the metallic substrate, as well as fluorine due to the use of hexafluorozirconic acid solution. In the case of Fe^{3+} and Cu^{2+} modified conversion solutions, small amounts of these elements can also be detected in the coating (~ 2-7 at.%).

Previous studies showed that native zinc and aluminum oxide layers on the HDG sample surface can be dissolved by "free" fluoride ions as shown in reactions (1) and (2) [14,34]:

$$3\ Zn^{2+} + ZrF_6^{2-} \rightarrow 3\ ZnF_2 + Zr^{4+} \quad (1)$$

$$Al^{3+} + ZrF_6^{2-} \rightarrow AlF_6^{3-} + Zr^{4+} \quad (2)$$

Figure 1 shows the XPS spectra of Zr (the spectra of all other samples are similar, but not shown here) on a polished and pretreated zinc substrate of high-purity. Obtained position of the Zr 3d peak corresponds well with values reported for Zr^{4+} in ZrO_2 in other studies (Zr

$3d_{3/2}$: 185.3 – 184.8 eV, Zr $3d_{5/2}$: 182.4 – 183.7 eV). Moreover the XPS results support the ToF-SIMS data, which shown ZrO^+ as an ion (see section 3.2). [18,27,32,33].

Regarding to the formation mechanism of the zirconium oxide layer, Lunder et al. [14] showed that the layer growth starts with hydrogen evolution and oxygen reduction in the near surface induced by acidic dissolution of zinc accordingly to reactions (3) and (4):

$$2\ H^+ + 2\ e^- \rightarrow H_2 \uparrow \quad (3)$$

$$O_2 + 2\ H_2O + 4\ e^- \rightarrow 4\ OH^- \quad (4)$$

Consequently, the interface alkalization leads to the formation of ZrO_2 containing conversion coatings as shown in reaction (5) [34]:

$$ZrF_6^{2-} + 4\ H_2O \rightarrow ZrO_2 \bullet H_2O + 6\ HF + O^{2-} \quad (5)$$

The oxygen to zircon concentration ratio (c_O/c_{Zr}) was found to be in the range from 3 to 7.7, which exceeds the expected value for a stoichiometrical zirconium oxide layer. The deviation from the expected values may partially originate from oxygen containing organic adsorbents present at the conversion layer surface. Additionally, the hydration of the zirconium oxide may also lead to observed deviation from the expected value (see eqn. (5)).

The effect of the additives on the growth kinetics can clearly be seen in Figure 2. Using identical immersion times, the copper-doped conversion solution lead to the thickest coatings on the substrate, whereas dipping in to the iron-dopped conversion bath and the original conversion solution lead to formation thinner layers. In contrast to the other samples, the HZF+Cu specimen showed a large scattering in the thickness of the conversion coating. This is related to an inhomogeneous precipitation of the zircon oxide layer on the metallic substrate and is clearly exhibited in the corresponding micrographs (see section 3.3 & 3.4). Andreatta et al. showed that the zirconium oxide layer is preferentially deposited at the cathodic areas on

the surface of the metallic substrate [19]. It is assumed, that the Cu^{2+} and Fe^{3+} ions in the conversion solution are reduced to their metallic states on the HDG substrate. The electrons used for this reduction reaction originate from the dissolution of zinc during the etching process:

$$3\ Zn + 2\ Fe^{3+} \rightarrow 3\ Zn^{2+} + 2\ Fe \downarrow \quad (6)$$

$$Zn + Cu^{2+} \rightarrow Zn^{2+} + Cu \downarrow \quad (7)$$

The presence of these local elements accelerates zinc corrosion process. The associated cathodic reactions of hydrogen evolution and oxygen reduction are accelerated at the deposited copper and iron micro cathodes. Based on these reactions, the local pH shift to higher values (alkalization) is amplified, constituting the more effective kinetics of growth of the zirconium oxide layer. The XPS sputter profiles in Figure 3 show the presence of small amounts of iron and copper within the conversion layer to support the suggested mechanism of acceleration. An enrichment of these elements within the coating or at the interface between the substrate and the conversion layer could not be observed. Similar observation was reported by Adhikari et al. [24].

3.2 Layer homogeneity of different conversion coatings after various immersion times

Figure 4 represents the lateral distribution of total and two selected secondary ion signals obtained by ToF-SIMS analysis performed in imaging-mode over 400 s on polished samples immersed for 60 s in different conversion solutions (conversion solution, Fig. 4b; conversion solution with addition of Fe^{3+}, Fig. 4c; conversion solution with addition of Cu^{2+}, Fig. 4d). An uncoated HDG sample was used as a reference (Fig. 4a). Regarding the high sensitivity of this technique, trace amounts of Al remained after the alkaline cleaning process are clearly visible and were chosen as a reference signal.

The ToF-SIMS images of samples immersed in conversion solutions indicate a more or less continuous zirconium oxide layer at the uppermost sample surface. Fig. 4b shows higher aluminium intensities at the zinc grain boundaries. Additionally, another indication for a continuous ZrO_2 layer formation is a significant decay of the aluminium signal originally present in the case of cleaned HDG sample. To investigate the influence of immersion time on the chemical composition and characteristic properties of conversion layers HDG samples were immersed for 5 seconds in same conversion solutions as previously discussed. Figure 5 shows the signal intensities for ZrO^+ and Al^+ secondary ion signals for all analysed samples and for both immersion times (5 s and 60 s). The ZrO^+ signal is corrected with the signal for a sulphur containing contaminant. This contaminant-peak partly overlaps with the ZrO^+ peak. The ZrO^+ signal intensities, for all coated samples presented in figure 5, are several orders of magnitudes higher than on the reference sample. The samples immersed for 5 s show slightly lower ZrO^+ signal intensities. Longer reaction times and thicker layers do not change the signal intensity significantly. The Al^+ signal intensity is clearly reduced with growing reaction times due to the formation of thicker ZrO_2 surface layer. Regarding the high surface sensitivity (1-3 monolayers) of ToF-SIMS, these results indicate the presence of a continuous layer, which was impossible to be shown using other analytical methods. Additionally, small amounts of metallic zinc were also detected in ZrO_2 surface layer.

3.3 Surface morphology of modified zirconium oxide conversion layer

To investigate the surface morphology of different zirconium based oxide coatings in more detail, FE-SEM microscopy studies were performed. Figure 6 shows FE-SEM images of polished HDG-surfaces after treatment with different conversion coatings at various conversion times (figure 6). Figure 6a illustrates the surface morphology of an cleaned and polished HDG reference sample. The micro-scratches from the polishing procedure are clearly visible. After 60 s immersion in the undoped H_2ZrF_6-pretreatment solution (Fig. 6b),

the surface structure of polished HDG substrate is still visible, indicating that the formed oxide layer is too thin to significantly change the surface morphology of the substrate. In comparison to the standard conversion solution, immersion of the substrate in Fe^{3+}- modified conversion solution leads to a thicker conversion layer under equivalent immersion times (Fig. 6d). In agreement with other studies, agglomerates of ZrO_2-nodules were also observed [24]. In contrast, addition of Cu^{2+} to the conversion solution leads to an inhomogeneous zirconium oxide layer precipitation as it can be seen in figure 6f and 6g. Due to the low lateral resolution of the ToF-SIMS, obtained results could not confirm the data obtained using FE-SEM. We believe that the deposition of the conversion layer preferentially starts at the copper micro cathodes and following by lateral growth around these sites. Similar results were reported from other authors on different substrates [14,15,19]. Furthermore, due to detection limitation of the FE-SEM, clear identification of reduced copper on the surface is not possible. However, in comparison to HZF and HZF+Fe conversion solution the surface of the HDG substrate was not completely covered after immersion for 60 s.

After 300 s immersion time (Fig. 6c, 6e, 6h) differences between the various conversion solutions became more evident. Coating of HDG samples in undoped and Fe^{3+} modified conversion solutions led to formation of dense layer on the substrate surface and surface scratches from the metallic substrate were no longer observable. In contrast to preceding investigations from other authors [35], the formation of micro-cracks resulting from the dehydration process or due to residual stress caused by the non-uniform thickness of the films were observed. Additionally, both surfaces were covered with small nodules with a diameter between 20 and 250 nm. Moreover, figure 6h confirmed the significant effect of the copper additive to the conversion solution on the kinetic of the film growth. The substrate surface was completely covered after 300 s in the HZF+Cu conversion bath and appeared smoother compared to figure 6c and 6e. These observations agree well with data about the coating thickness as determined by XPS (Fig. 2). Furthermore, the size of formed metal oxide

particles, which was found to be in the range from 20 nm to 1 µm, also increased. As a result of increased film thickness, numerous micro-cracks in the conversion coating were observed (Fig. 6h). It is not clear whether the cracks occurred during the dehydration process or resulted from the residual stress by non-uniform film thickness.

3.4 In-situ corrosion potential measurements

To *in-situ* monitor the film formation in different conversion solutions measurements of corrosion potential (open-circuit potential, OCP) on immersed HDG sample were performed. Figure 7 represents the open-circuit-potentials (OCP) of alkaline cleaned HDG-substrates immersed in different conversion solutions. During the first 5 - 8 seconds (grey area in Fig. 7) OCP values of all immersed samples were decreasing. This can be interpreted by following simplified model. On the one hand, the native Al- and Zn-oxyhydroxide layers were dissolved by the acidic conditions in the conversion solution coinciding with an "active corrosion behaviour" of the metallic substrate [36]. On the other hand, the presence of fluoride species in the conversion solution shifts the OCP to more negative values compared to a fluoride free solution because of formation of zinc flouride (section 3.1, eqn. (1) and (2)):

$$Zn \rightarrow Zn^{2+} + 2\ e^{-} \qquad \text{(electrode reaction)} \qquad (8)$$

$$3\ Zn^{2+} + ZrF_6^{2-} \rightarrow 3\ ZnF_2 + Zr^{4+} \qquad \text{(zinc fluoride)} \qquad (1)$$

$$3\ Zn + ZrF_6^{2-} \rightarrow 3\ ZnF_2 + Zr^{4+} + 2\ e^{-} \qquad \text{(net electrode reaction)} \qquad (9)$$

In the case of the undoped conversion solution, the OCP value slightly increased to -0.811 V_{SHE} after decreasing to a minimum value of -0.817 V_{SHE} after 8 s. If the conversion solution contained iron or copper, the OCP principally shifted to more positive values compared to the undoped conversion solution (e.g. local minimum after 6 s was -0.803 V_{SHE} for HZF+Fe and -0.775 V_{SHE} after 8 s for HZF+Cu conversion solution, respectively). This is due to a reduction of Fe^{3+} or Cu^{2+} ions on the surface during the conversion process (eqn. (6)

and (7)) resulting in a more positive mixed potential of electrochemical equilibrium of Zn and Fe or Zn and Cu containing sample surface, respectively (see eqn. (10) and (11)).

The driving force (electromotive force, EMF) for iron or copper reduction can be estimated by Nernst equations of a copper and iron electrode under the assumption of cuprous copper and ferric iron:

$$\varepsilon(Fe/Fe^{3+}) = \varepsilon^{\circ}(Fe/Fe^{3+}) + R \cdot T / 3 \cdot F \cdot \ln a(Fe^{3+})/a(Fe) \quad (10)$$

$$= -0.746\ V_{SHE}$$

where R is the gas constant and F is the Faraday constant, with $a(Fe) \approx 1$, $a(Fe^{3+}) \approx c(Fe^{3+})/c^{\circ}$ with $c^{\circ} = 1$ mol/L, $c(Fe^{3+}) = 0{,}1$ mmol/L, $\varepsilon^{\circ}(Fe/Fe^{3+}) = +0.036\ V_{SHE}$ (taken from [37]),

$$\varepsilon(Cu/Cu^{2+}) = \varepsilon^{\circ}(Cu/Cu^{2+}) + R \cdot T / 2 \cdot F \cdot \ln a(Cu^{2+})/a(Cu) \quad (11)$$

$$= -0.133\ V_{SHE}$$

where R is the gas constant and F is the Faraday constant, with $a(Cu) \approx 1$, $a(Cu^{2+}) \approx c(Cu^{2+})/c^{\circ}$ with $c^{\circ} = 1$ mol/L, $c(Cu^{2+}) = 0{,}1$ mmol/L, $\varepsilon^{\circ}(Cu/Cu^{2+}) = +0.340\ V_{SHE}$ (taken from [37]).

Measurement of the OCP in conversion solution without Fe^{3+} or Cu^{2+} ions provided an electrode potential of Zn/Zn^{2+} of around -0.80 V_{SHE}. This is around 0.05 V or 0.67 V more negative than the electrode potentials of Fe/Fe^{3+} or of Cu/Cu^{2+} redox couples, respectively, resulting in a more positive mixed potential in the case of Fe^{3+} or Cu^{2+} ions containing conversion solutions.

The EMF for copper reduction (eqn. (7)) is around 0.60 V higher than for iron reduction (eqn. (6)). This results presumably in a higher slope of the OCP vs. time plots in the case of Fe^{3+} or Cu^{2+} ions containing conversion solutions in the time period directly after the local minimum

and the end of grey colored area, where the reduction reactions of Fe^{3+} or Cu^{2+} are dominant. Thus the following ranking of the OCP vs. time plot-slopes was observed:

Cu^{2+} doped HFZ >> Fe^{3+} doped HZF > undoped HZF

Deposition of iron or copper on the substrate surface generates local cathodic areas where hydrogen and hydroxyl ions are preferentially generated. Most probably because of the higher EMF (potential difference) between the zinc surface and the copper micro cathodes, the required cathodic reactions (pH shifting reactions eqn. (3) and (4)) for ZrO_2 precipitation mainly take place at the deposited copper. This leads to non-uniform ZrO_2 layer precipitation as shown in SEM micrographs (Fig. 6g). In contrast to that, the EMF between the zinc surface and the iron cathodes is significantly lower and the local alkalization occurs on the micro cathodes as well as on the zinc surface. This coincides with previously discussed SEM micrographs (Fig. 6d). Additionally, enhanced kinetics of oxygen reduction reaction on copper relative to iron may play an important role in shifting of pH value in alkaline direction.

Between 8 and 600 seconds the OCP value of all samples became nearly time independent indicating that an electrochemical equilibrium between the substrate and the conversion solution (eqn. (1)-(5) and (10)) was achieved (for the undoped conversion solution after ~ 30 s and for the iron or copper doped conversion solution after ~ 500 s or 400 s, respectively). This coincides with XPS measurements indicating no more significant thickness growth of the conversion layer with increased immersion time.

In the iron doped conversion solution the film formation was slowing down after 25 s, indicated by the change in the slope of the OCP curve. In case of copper as doping element, the slope of the OCP vs. time plot was significantly higher compared to iron doped solution and did not decrease until approximately 170 s. This implies the highest deposition rate of the zirconium oxide conversion layer among all tested conversion solutions. Afterwards, change

in the slope of the OCP curve was observed indicating decrease of the deposition rate. A time independent behaviour was evident after ~ 400 s when the film thickness reached a maximum.

In summary, the kinetics of the pH shifting reactions on iron or copper micro cathodes is higher than that on a zinc surface without deposited iron or copper [38]. This results in an enhancement of the conversion layer growth kinetics and increased thickness. This correlates well with discussed behaviour of slopes of different OCP vs. time plots on the one hand and time independent OCP values and XPS depth profiles on the other hand.

3.4 Potentiodynamic polarization curves

Potentiodynamic polarization scans in oxygen aerated 0.1 M Na_2SO_4 solution were performed to evaluate the corrosion current density measured on samples immersed in different conversion solutions for different times. Figure 8 summarizes results of these measurements. The corrosion current density decreases up to 95 % in the case of coated specimens in comparison to the untreated, alkaline cleaned sample (47.9 ± 3.4 µA/cm²) indicating reduced kinetics of corrosion reactions at the interface between specimen and electrolyte.

With longer immersion times the current densities measured on samples immersed in HZF and HZF+Fe conversion solutions slightly increased for deposition times between 60 s (i_{corr}=1.1 ± 0.1 µA/cm²) and 300 s (i_{corr}=2.5 ± 0.1 µA/cm²). However, after a relative short immersion time a significant decrease in the corrosion current density already occurs. This is an essential aspect for a continuous industrial application of these conversion pretreatments because of short deposition times.

Figure 9 represent polarization curves of all investigated samples immersed in different conversion solutions for 60, 90, 180 and 300 s. Compared to cleaned samples, the corrosion potential of HDG samples immersed in HZF and HZF+Fe conversion solutions shifted to more negative values as well as the oxygen reduction current was also reduced. This indicates

a presence of a barrier effect caused by the conversion layer hindering diffusion of oxygen to the metallic sample surface leading to smaller oxygen reduction current and shift of the corrosion potential to more negative values. Similar effect was simulated by an analogous measurement (Fig. 9d) performed using an cleaned HDG sample after purging the electrolyte with N_2 to reduce oxygen concentration in the solution. Due to a reduced oxygen reduction current the delamination kinetics of an organic coated pretreated sample is retarded – Stratmann et al. previously showed that the determining step of the delamination kinetics is the oxygen reduction current followed by alkalization of the interface between organic coating and metallic substrate [39].

In the case of polarization curves recorded on sample immersed in HZF+Cu conversion solution a similar reduction of the corrosion current densities has not been observed which is in agreement with the micrographs and the *in-situ* corrosion potential measurements (Fig. 7). After short immersion times (e.g. 60 s) the zirconium oxide layer growth was truncated on the deposited copper micro cathodes deposited on the zinc substrate. This leads to residual uncoated areas at the local zinc anodes and thus to a smaller barrier effect concerning corrosion current density or oxygen reduction. With longer immersion times the ZrO_2 deposition continued at extended areas surrounding the micro cathodes, but the barrier effect increased only slightly indicated by a relative small decrease of measured corrosion current densities. Moreover, the zircon oxide layer deposited for longer immersion times (300 s) was most likely defective as discussed above (Fig. 6h). Thus, independent of coating thickness, the copper modified conversion layer is less effective in corrosion protection than both other conversion solutions.

4. Conclusion

$Fe(NO_3)_3 \cdot 9H_2O$ and $Cu(NO_3)_2 \cdot 3H_2O$ modified zirconium-based conversion solutions were used to deposit Zr-based conversion layer on line produced non-temper rolled galvanized steel (HDG) substrates. Various electrochemical and surface analytical methods were applied to investigate the chemical composition and electrochemical properties of resulting layers. Based on the surface characterization by XPS and ToF-SIMS the chemical composition of the conversion layer was investigated and the main component is zirconium oxide (ZrO_2). Small amounts of additives and zinc from the substrate were also detected in the coating. By in-situ corrosion potential measurements an increase of the potential during the pretreatment procedure in the conversion solution was clearly shown. In case of Fe^{3+} or Cu^{2+} cations in the conversion solution, the OCP shifted to more positive values because of generation of Fe or Cu micro cathodes. The time dependence of the OCP correlates well with the resulting layer growth process. Potentiodynamic polarization measurements performed on HDG samples immersed in HZF and HZF+Fe conversion solutions showed a significant decrease of the corrosion current density already after short immersion times. In agreement to the ToF-SIMS images, this indicates a continuous barrier layer present on the substrate surface. In the case of HZF+Cu conversion solution a comparable barrier effect could not be observed using FE-SEM and electrochemical measurements. This can be explained by a non-uniform ZrO_2 layer participation and cracks present in the coating layer. It was shown, that both HZF and HZF+Fe conversion solutions have potential for application in a continuous industrial production line offering compact protective layers with good protection properties against corrosion process.

Acknowledgements

Authors gratefully acknowledge Stefanie Wierhake for the supporting XPS and AFM measurements and Kay Kämmerer for performing all SEM investigations. Moreover, the authors would like to thank Thomas Sondermann and Christoph Strahl from alufinish Gmbh & Co KG for offering materials and helpful discussions. Furthermore, authors express their cordially thanks to Linda Luxem for language revision of the manuscript.

References

[1] Agency for Toxic Substance, U.S. Public Health Service, Toxicological Profile for Chromium, ATDSRyTP-88y10, 1989.

[2] M.G.S. Ferreira, R.G. Duarte, M.F. Montemor, A.M.P. Simões, Silanes and rare earth salts as chromate replacers for pre-treatments on galvanised steel, Electrochimica Acta 49 (2004) 2927.

[3] A. Franquet, C. Le Pen, H. Terryn, J. Vereecken, Effect of bath concentration and curing time on the structure of non-functional thin organosilane layers on aluminium, Electrochimica Acta 48 (2003) 1245.

[4] M.-G. Olivier, M. Fedel, V. Sciamanna, C. Vandermiers, C. Motte, M. Poelman, F. Deflorian, Study of the effect of nanoclay incorporation on the rheological properties and corrosion protection by a silane layer, Progress in Organic Coatings 72 (2011) 15.

[5] D. Wang, G.P. Bierwagen, Sol–gel coatings on metals for corrosion protection, Progress in Organic Coatings 64 (2009) 327.

[6] D. Zhu, W.J. van Ooij, Enhanced corrosion resistance of AA 2024-T3 and hot-dip galvanized steel using a mixture of bis-[triethoxysilylpropyl]tetrasulfide and bis-[trimethoxysilylpropyl]amine, Electrochimica Acta 49 (2004) 1113.

[7] M.A. Arenas, M. Bethencourt, F.J. Botana, J. de Damborenea, M. Marcos, Inhibition of 5083 aluminium alloy and galvanised steel by lanthanide salts, Corrosion Science 43 (2001) 157.

[8] N.C. Rosero-Navarro, M. Curioni, R. Bingham, A. Durán, M. Aparicio, R.A. Cottis, G.E. Thompson, Electrochemical techniques for practical evaluation of corrosion inhibitor effectiveness. Performance of cerium nitrate as corrosion inhibitor for AA2024T3 alloy, Corrosion Science 52 (2010) 3356.

[9] E. Almeida, T.C. Diamantino, M.O. Figueiredo, C. Sá, Oxidising alternative species to chromium VI in zinc galvanised steel surface treatment. Part 1—A morphological and chemical study, Surface and Coatings Technology 106 (1998) 8.

[10] H. Li, K. Liang, L. Mei, S. Gu, S. Wang, Corrosion protection of mild steel by zirconia sol-gel coatings, Journal of Materials Science Letters 20 (2001) 1081-1083.

[11] G. Gusmano, G. Montesperelli, M. Rapone, G. Padeletti, A. Cusmà, S. Kaciulis, A. Mezzi, R. Di Maggio, Zirconia primers for corrosion resistant coatings, Surface and Coatings Technology 201 (2007) 5822.

[12] R. Di Maggio, L. Fedrizzi, S. Rossi, Effect of the chemical modification of the precursor of ZrO2 films on the adhesion of organic coatings, Journal of Adhesion Science and Technology 15 (2001) 793.

[13] L. Fedrizzi, F.J. Rodriguez, S. Rossi, F. Deflorian, R. Di Maggio, The use of electrochemical techniques to study the corrosion behaviour of organic coatings on steel pretreated with sol–gel zirconia films, Electrochimica Acta 46 (2001) 3715.

[14] O. Lunder, C. Simensen, Y. Yu, K. Nisancioglu, Formation and characterisation of Ti–Zr based conversion layers on AA6060 aluminium, Surface and Coatings Technology 184 (2004) 278.

[15] J.H. Nordlien, J.C. Walmsley, H. Østerberg, K. Nisancioglu, Formation of a zirconium-titanium based conversion layer on AA 6060 aluminium, Surface and Coatings Technology 153 (2002) 72.

[16] O. Lunder, F. Lapique, B. Johnsen, K. Nisancioglu, Effect of pre-treatment on the durability of epoxy-bonded AA6060 aluminium joints, International Journal of Adhesion and Adhesives 24 (2004) 107.

[17] P. Laha, T. Schram, H. Terryn, Use of spectroscopic ellipsometry to study Zr/Ti films on Al, Surf. Interface Anal. 34 (2002) 677.

[18] D. Chidambaram, C.R. Clayton, G.P. Halada, The role of hexafluorozirconate in the formation of chromate conversion coatings on aluminum alloys, Electrochimica Acta 51 (2006) 2862.

[19] F. Andreatta, A. Turco, I. de Graeve, H. Terryn, J.H.W. de Wit, L. Fedrizzi, SKPFM and SEM study of the deposition mechanism of Zr/Ti based pre-treatment on AA6016 aluminum alloy, Surface and Coatings Technology 201 (2007) 7668.

[20] P. Puomi, H.M. Fagerholm, J.B. Rosenholm, K. Jyrkäs, Comparison of different commercial pretreatment methods for hot-dip galvanized and Galfan coated steel, Surface and Coatings Technology 115 (1999) 70.

[21] P. Puomi, H.M. Fagerholm, J.B. Rosenholm, R. Sipilä, Optimization of commercial zirconic acid based pretreatment on hot-dip galvanized and Galfan coated steel, Surface and Coatings Technology 115 (1999) 79.

[22] S. Verdier, N. van der Laak, F. Dalard, J. Metson, S. Delalande, An electrochemical and SEM study of the mechanism of formation, morphology, and composition of titanium or zirconium fluoride-based coatings, Surface and Coatings Technology 200 (2006) 2955.

[23] C. Stromberg, P. Thissen, I. Klueppel, N. Fink, G. Grundmeier, Synthesis and characterisation of surface gradient thin conversion films on zinc coated steel, Electrochimica Acta 52 (2006) 804.

[24] S. Adhikari, K.A. Unocic, Y. Zhai, G.S. Frankel, J. Zimmerman, W. Fristad, Hexafluorozirconic acid based surface pretreatments: Characterization and performance assessment, ADVANCES IN CORROSION SCIENCE FOR LIFETIME PREDICTION AND SUSTAINABILITYSelection of papers from the 8th ISE Spring Meeting2-5 May 2010, Columbus, OH, USA 56 (2011) 1912.

[25] F.O. George, P. Skeldon, G.E. Thompson, Formation of zirconium-based conversion coatings on aluminium and Al–Cu alloys, Corrosion Science 65 (2012) 231.

[26] W. Warnecke, R. Bode, R. Kothe, L. Meyer, Modernes Feuerverzinktes Feinblech-Herstellung; Aufbau der Überzüge und Verarbeitungseigenschaften, Thyssen Technische Berichte 1 (1991).

[27] H. Ardelean, I. Frateur, P. Marcus, Corrosion protection of magnesium alloys by cerium, zirconium and niobium-based conversion coatings, Corrosion Science 50 (2008) 1907.

[28] S. Le Manchet, D. Verchère, J. Landoulsi, Effects of organic and inorganic treatment agents on the formation of conversion layer on hot-dip galvanized steel: An X-ray photoelectron spectroscopy study, Thin Solid Films 520 (2012) 2009.

[29] H. Eivaz Mohammadloo, A.A. Sarabi, A.A. Sabbagh Alvani, H. Sameie, R. Salimi, Nano-ceramic hexafluorozirconic acid based conversion thin film: Surface characterization and electrochemical study, Surface and Coatings Technology 206 (2012) 4132.

[30] L.R.F. Allen J. Bard, Electrochemical Methods: Fundamentals and Applications, Wiley, John & Sons, Incorporated, 2001.

[31] N. Fink, B. Wilson, G. Grundmeier, Formation of ultra-thin amorphous conversion films on zinc alloy coatings: Part 1. Composition and reactivity of native oxides on ZnAl (0.05%) coatings, Electrochimica Acta 51 (2006) 2956.

[32] W. Bensch, O. Helmer, M. Muhler, H. Ebert, M. Knecht, Experimental and Theoretical Bandstructure of the Layer Compound ZrSiTe, J. Phys. Chem. 99 (1995) 3326.

[33] Y.M. Wang, Y.S. Li, P.C. Wong, K.A.R. Mitchell, XPS studies of the stability and reactivity of thin films of oxidized zirconium, Applied Surface Science 72 (1993) 237.

[34] P. Taheri, K. Lill, J.H.W. de Wit, J.M.C. Mol, H. Terryn, Effects of Zinc Surface Acid-Based Properties on Formation Mechanisms and Interfacial Bonding Properties of Zirconium-Based Conversion Layers, J. Phys. Chem. C 116 (2012) 8426.

[35] X. Zhang, W.G. Sloof, A. Hovestad, E.P.M. van Westing, H. Terryn, J.H.W. de Wit, Characterization of chromate conversion coatings on zinc using XPS and SKPFM, Surface and Coatings Technology 197 (2005) 168.

[36] S.O. Klemm, J.-C. Schauer, B. Schuhmacher, A.W. Hassel, A microelectrochemical scanning flow cell with downstream analytics, Electrochimica Acta 56 (2011) 4315.

[37] Robert C. Weast (Ed.), Handbook of Chemistry and Physics, 50th ed., The Chemical Rubber CO., Cleveland, Ohio, 1969.

[38] E. McCafferty, Introduction to Corrosion Science, Springer New York, New York, 2010.

[39] M. Stratmann, R. Feser, A. Leng, Corrosion protection by organic films, Electrochimica Acta 39 (1994) 1207.

Figure captions

Table 1: Concentration of chemical elements present on the surface of the conversion layer as determined by XPS

Figure 1: Element XPS spectra of Zr recorded on polished high-purity zinc substrate after immersion of substrate in 1 mmol/l H_2ZrF_6 solution for 300 s at room temperature ($T \sim 20$ °C).

Figure 2: Film thickness of the different conversion layers at different immersion times determined by XPS sputter profiles. Reference sputter rate: $R(SiO_2) = 10$ nm/min.

Figure 3: XPS depth profiles recorded on samples treated in the Cu^{2+}-modified (denoted as HZF+Cu) or Fe^{3+}-modified (denoted as HZF+Fe) conversion solutions for 300 s. Reference sputter rate: $R(SiO_2) = 10$ nm/min.

Figure 4: TOF-SIMS element mappings performed on the surface of conversion coatings deposited on HDG samples by immersion in different conversion solutions. Presented are total counts (tc) and maximum counts per pixel (mc) of secondary ions, the Al^+- and the ZrO^+-signals for cleaned HDG sample (a), sample treated in HZF for 60 s (b), sample treated in HZF+Fe for 60 s (c) and sample treated in HZF+Cu for 60 s (d). Due to the comparable total counts, the ZrO^+-intensities are also comparable.

Figure 5: Comparison of numbers of counts recorded for ZrO^+ and Al^+ secondary ions during TOF-SIMS mapping performed on the surface of HDG samples immersed in different conversion solutions for 5 s and 60 s.

Figure 6: FE-SEM images of polished HDG samples after treatment with different conversion solutions for different conversion times: cleaned (a), in HZF for 60 s (b), in HZF

for 300 s (c), in HZF+Fe for 60 s (d), in HZF+Fe for 300 s (e), in HZF+Cu for 60 s (f), in HZF+Cu for 60 s (g) and in HZF+Cu for 300 s (h).

Figure 7: Open circuit potential measurements performed on the surface of alkaline cleaned HDG substrates during immersion of samples in different conversion solutions. The grey area is attributed to the dissolution of the native zinc and aluminum oxyhydroxide layers from the surface during the conversion treatment. The white area is allocated to the film formation of the conversion layer.

Figure 8: Comparison of corrosion current densities for HDG samples immersed in different conversion solutions for different times. Values of corrosion current densities were extrapolated from potentiodynamic polarization measurements using Tafel extrapolation method.

Figure 9: Potentiodynamic polarization curves of HDG samples, untreated (alkaline cleaned) and treated in different conversion solutions (the immersion times are indicated), recorded in 0.1 M Na_2SO_4. Following conversion solutions were used: undoped (a), HZF+Fe (b) and HZF+Cu (c). Figure 9d represent potentiodynamic polarization curve recorded on cleaned HDG sample immersed in oxygen aerated (solid line) and nitrogen purged (dashed line) 0.1 M Na_2SO_4 solution at $T \sim 20$ °C.

Table 1

element sample	O (at.%)	Zn (at.%)	Al (at.%)	Zr (at.%)	F (at.%)	Fe (at.%)	Cu (at.%)	c_O/c_{Zr}
untreated (alkaline cleaned)	60	29	11					
HZF 60s	60	8		19	13			3,1
HZF 300s	57	7		19	17			3
HZF+Fe 60s	69	6		13	9	3		5,2
HZF+Fe 300s	68	7		9	9	7		7,7
HZF+Cu 60s	66	8		18	6		2	3,7
HZF+Cu 300s	63	4		19	11		3	3,2

Figure 1

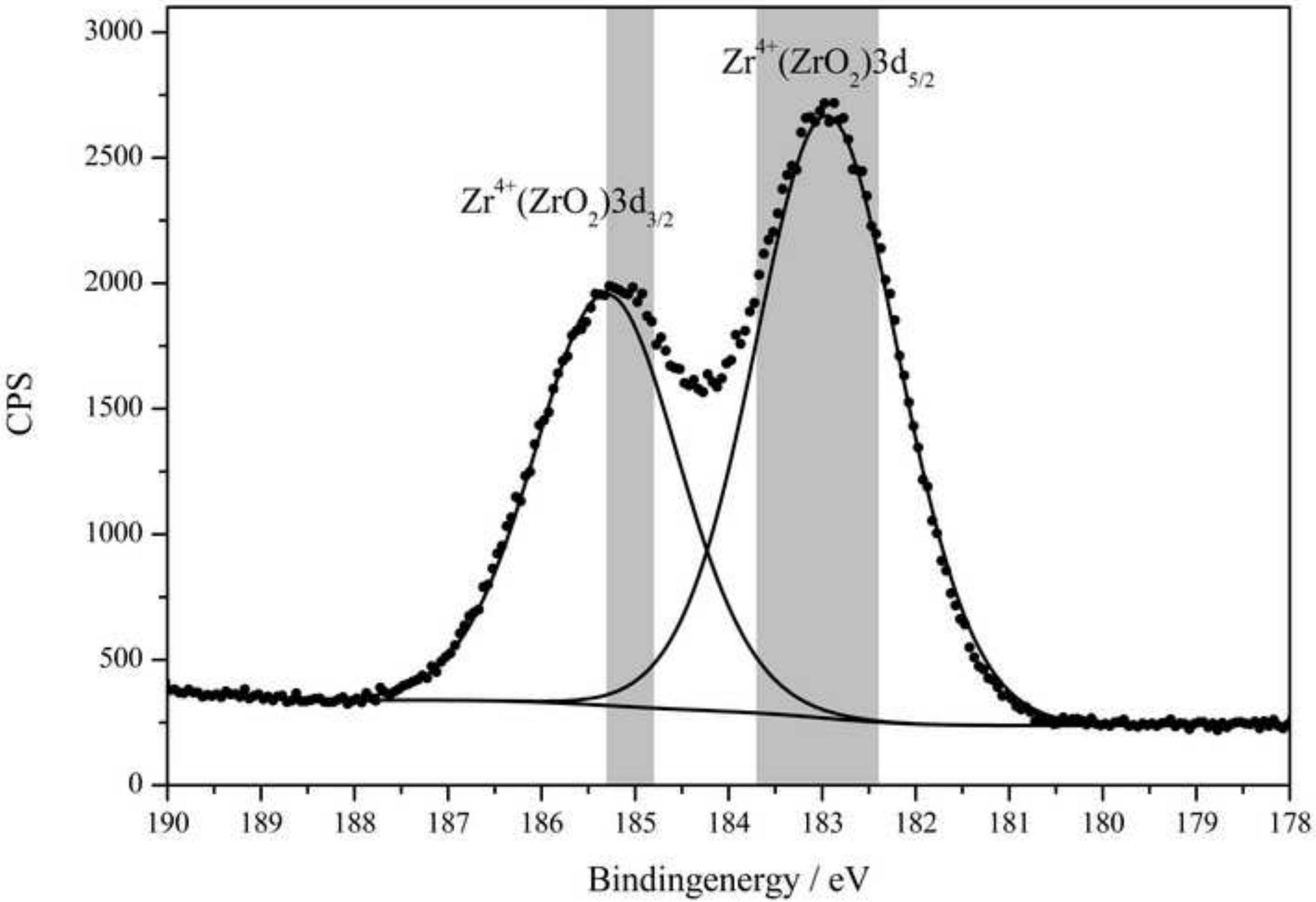
3000
2500
2000
1500
1000
500
0
CPS
190
189
188
187
186
185
184
183
182
181
180
179
178
Bindingenergy / eV
$Zr^{4+}(ZrO_2)3d_{5/2}$
$Zr^{4+}(ZrO_2)3d_{3/2}$

Figure 2

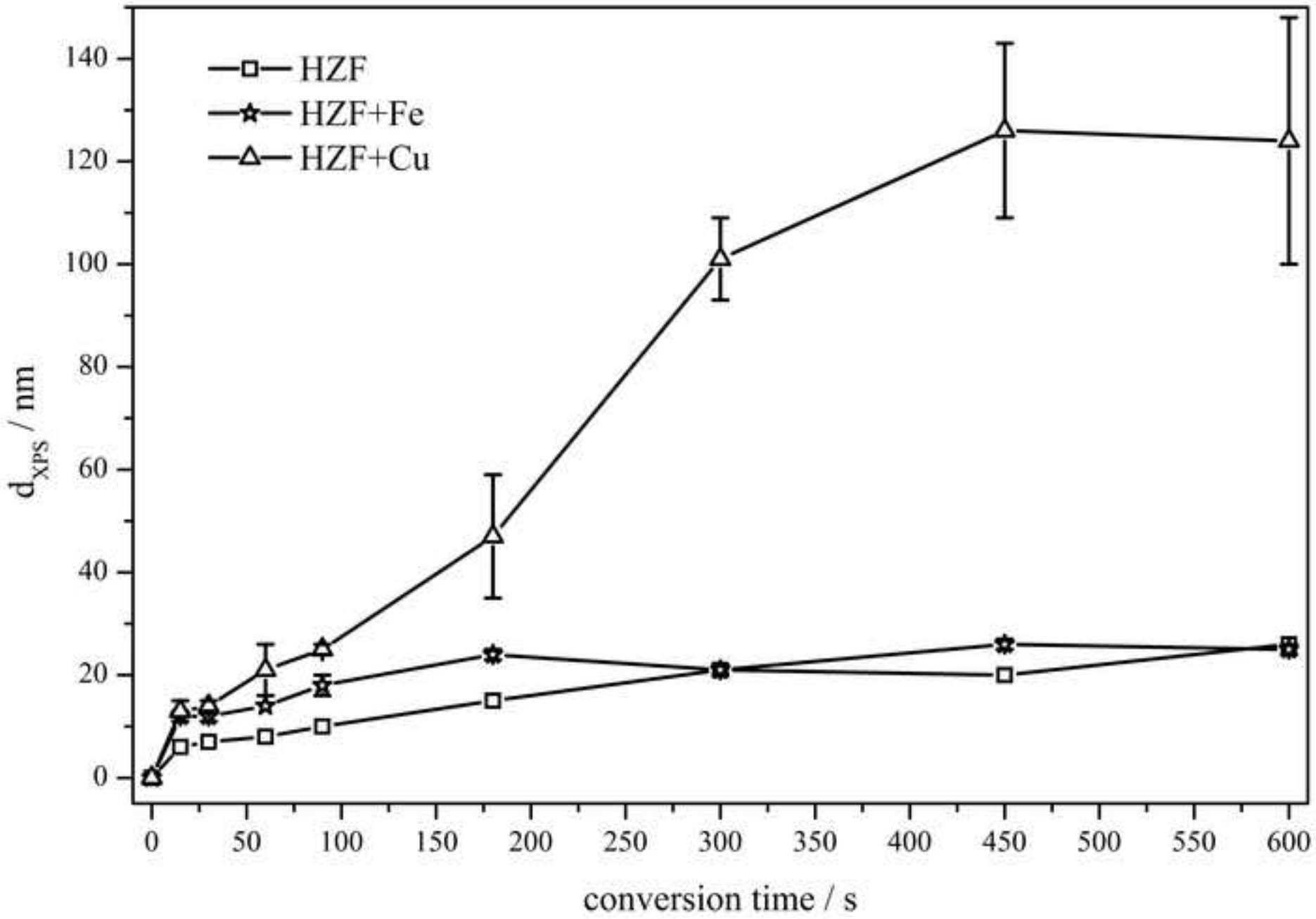
HZF
HZF+Fe
HZF+Cu
d_{XPS} / nm
conversion time / s
0
20
40
60
80
100
120
140
0
50
100
150
200
250
300
350
400
450
500
550
600

Figure 3

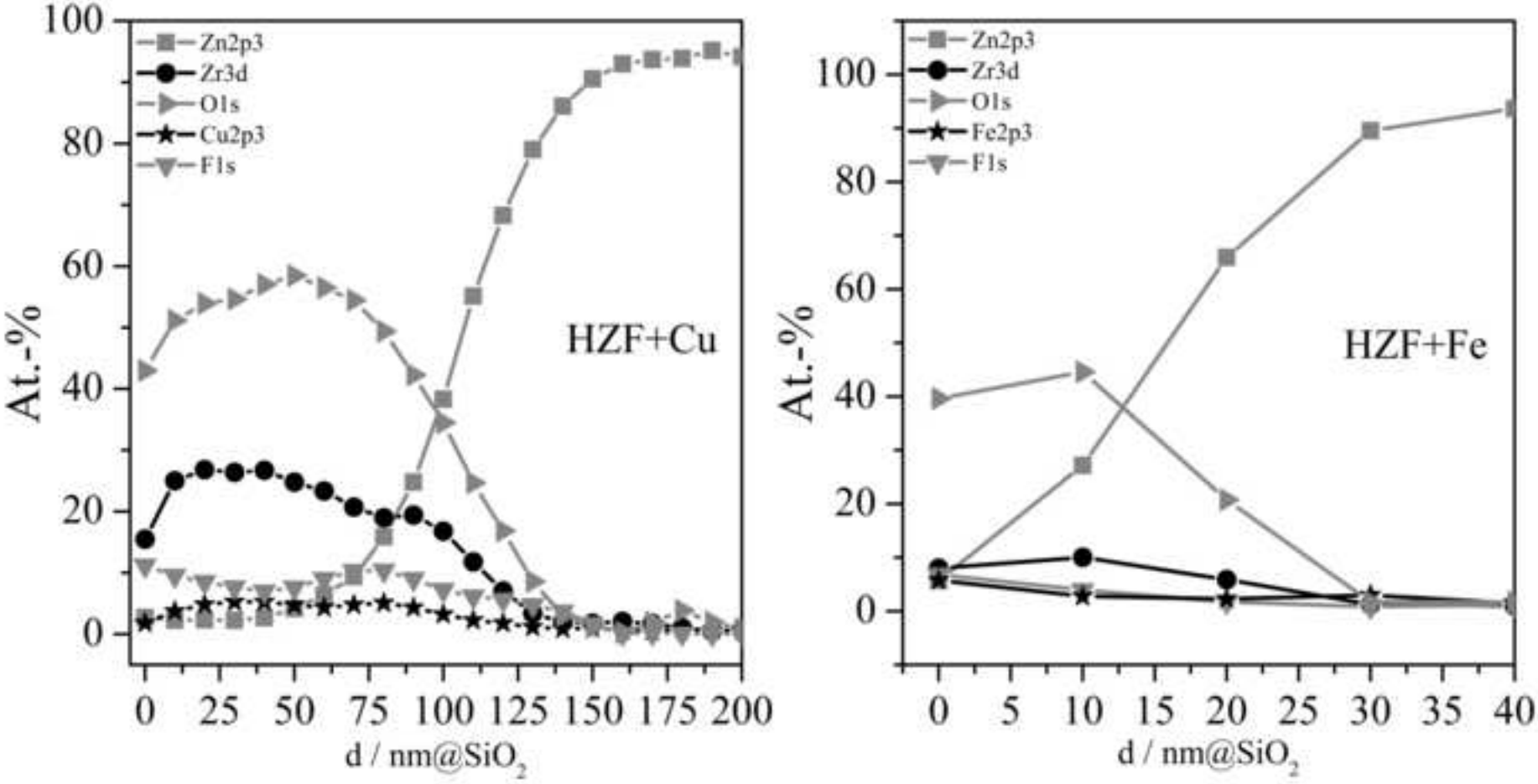
Zn2p3
Zr3d
O1s
Cu2p3
F1s
HZF+Cu
At.-%
d / nm@SiO2
Zn2p3
Zr3d
O1s
Fe2p3
F1s
HZF+Fe
At.-%
d / nm@SiO2

Figure 4

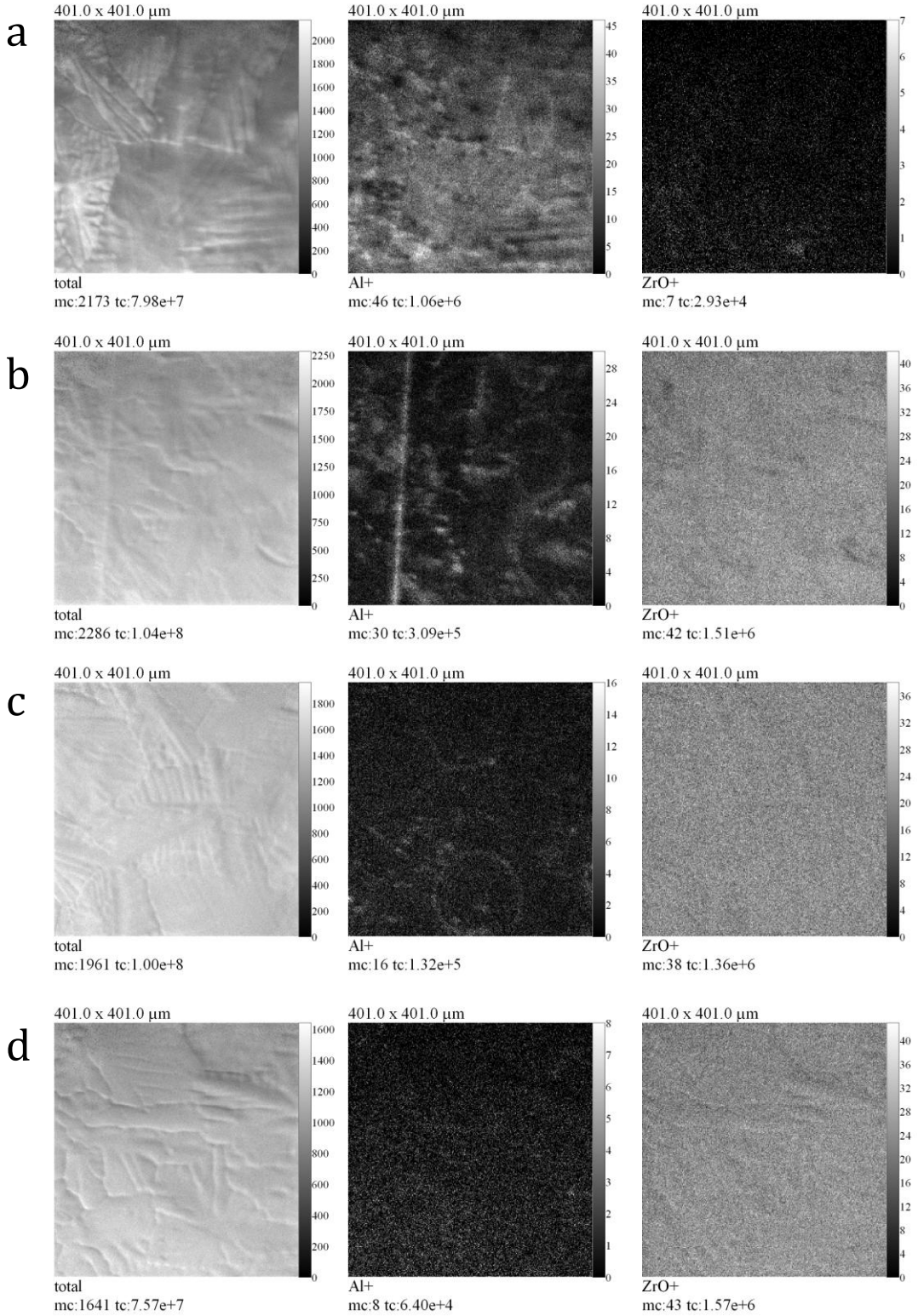
a
401.0 x 401.0 µm
total
mc:2173 tc:7.98e+7
401.0 x 401.0 µm
Al+
mc:46 tc:1.06e+6
401.0 x 401.0 µm
ZrO+
mc:7 tc:2.93e+4
b
401.0 x 401.0 µm
total
mc:2286 tc:1.04e+8
401.0 x 401.0 µm
Al+
mc:30 tc:3.09e+5
401.0 x 401.0 µm
ZrO+
mc:42 tc:1.51e+6
c
401.0 x 401.0 µm
total
mc:1961 tc:1.00e+8
401.0 x 401.0 µm
Al+
mc:16 tc:1.32e+5
401.0 x 401.0 µm
ZrO+
mc:38 tc:1.36e+6
d
401.0 x 401.0 µm
total
mc:1641 tc:7.57e+7
401.0 x 401.0 µm
Al+
mc:8 tc:6.40e+4
401.0 x 401.0 µm
ZrO+
mc:43 tc:1.57e+6

Figure 5

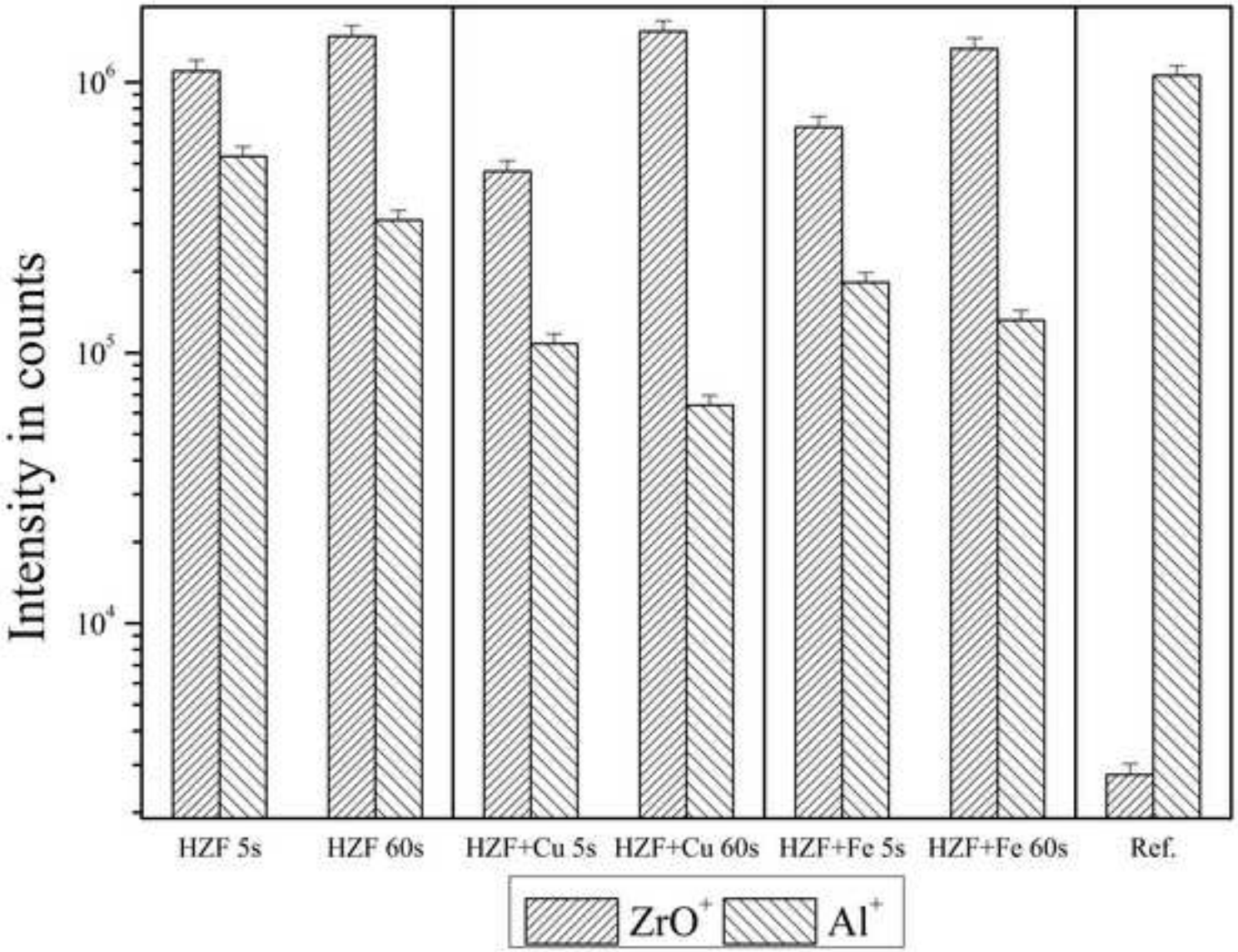
Intensity in counts
10^6
10^5
10^4
HZF 5s
HZF 60s
HZF+Cu 5s
HZF+Cu 60s
HZF+Fe 5s
HZF+Fe 60s
Ref.
ZrO^+
Al^+

Figure 6

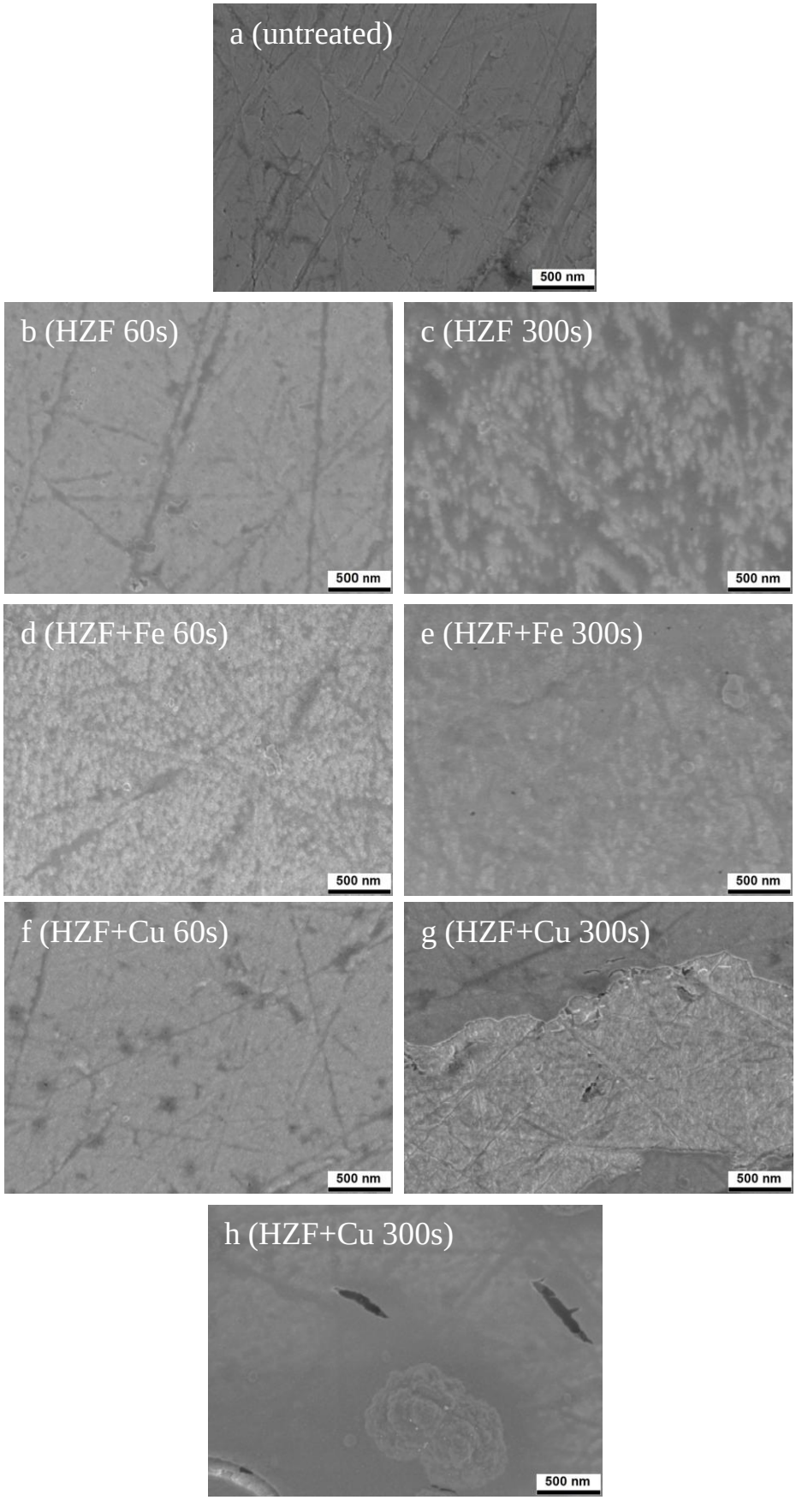
a (untreated)
500 nm
b (HZF 60s)
500 nm
c (HZF 300s)
500 nm
d (HZF+Fe 60s)
500 nm
e (HZF+Fe 300s)
500 nm
f (HZF+Cu 60s)
500 nm
g (HZF+Cu 300s)
500 nm
h (HZF+Cu 300s)
500 nm

Figure 7

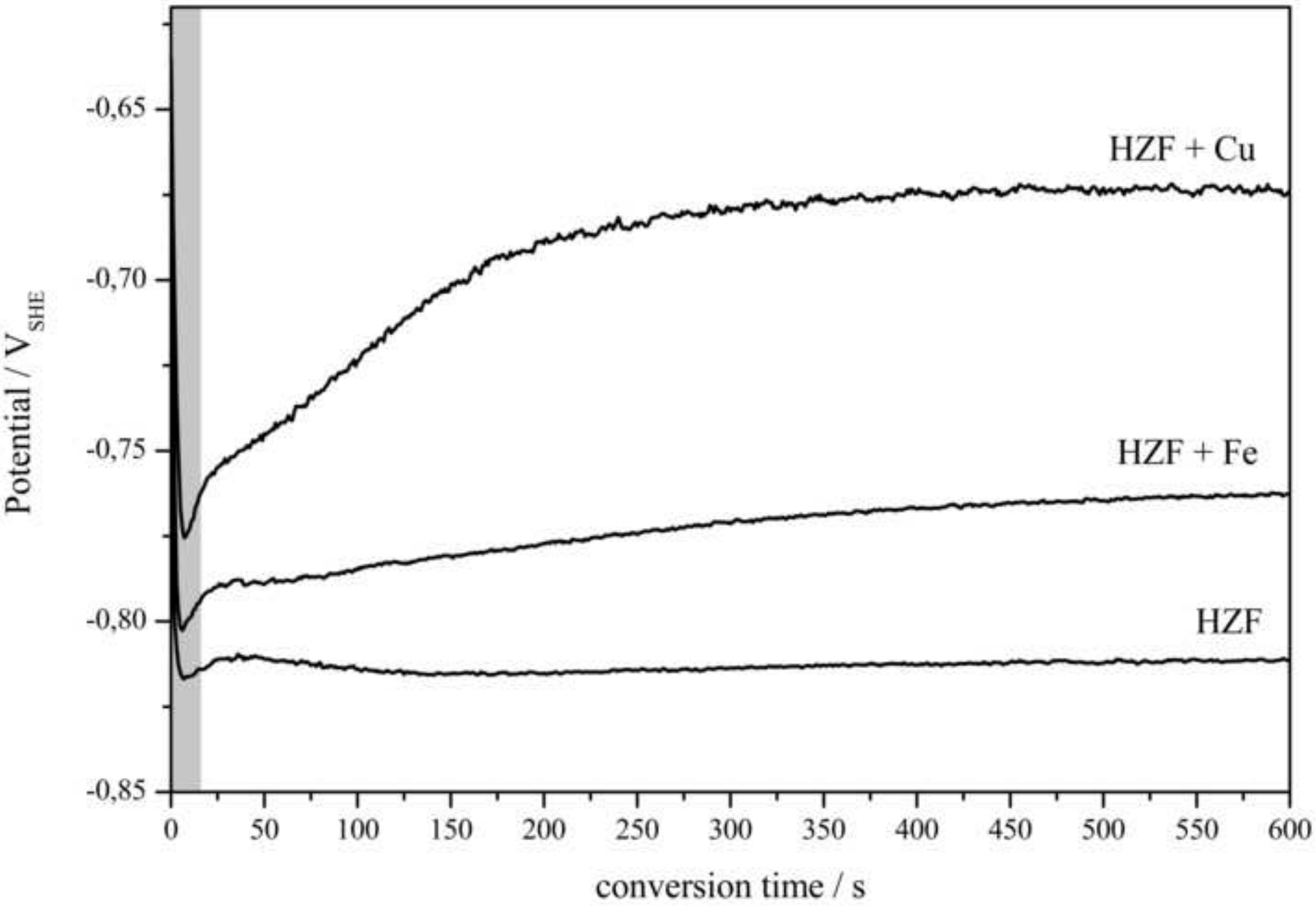
-0,65
-0,70
-0,75
-0,80
-0,85
Potential / V SHE
HZF + Cu
HZF + Fe
HZF
0
50
100
150
200
250
300
350
400
450
500
550
600
conversion time / s

Figure 8

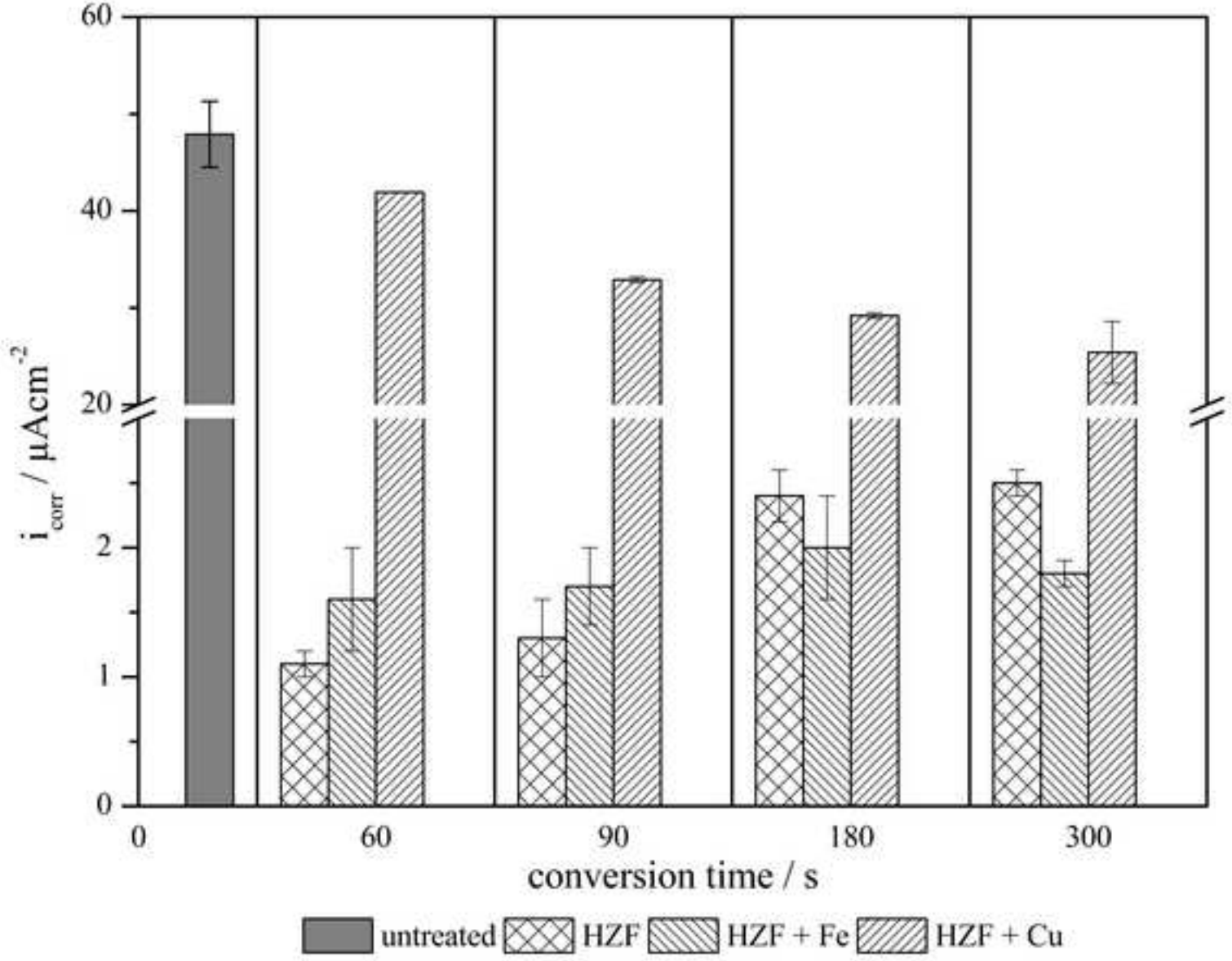
60
40
20
2
1
0
i_{corr} / μAcm^{-2}
0
60
90
180
300
conversion time / s
untreated
HZF
HZF + Fe
HZF + Cu

Figure 9

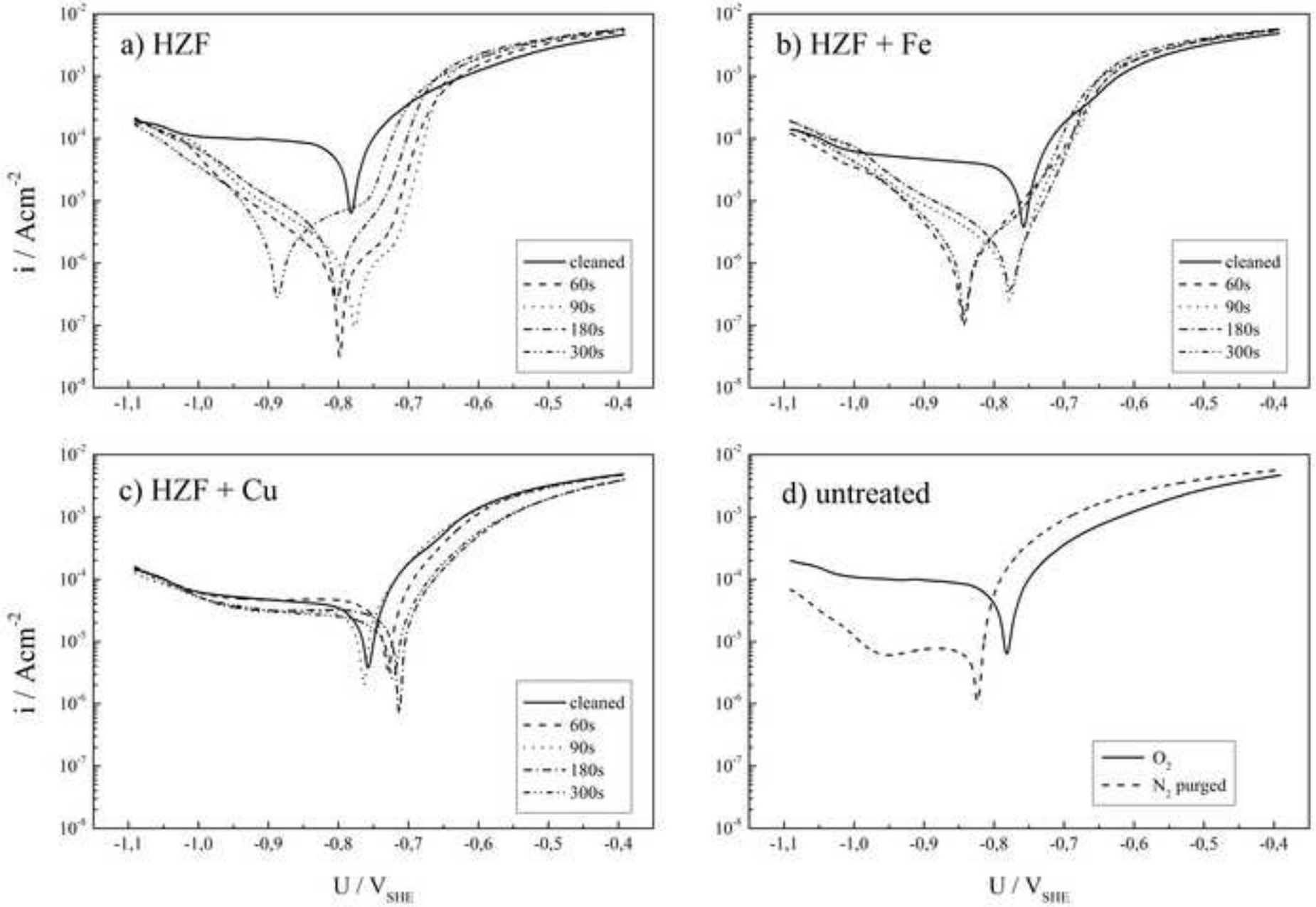
a) HZF
b) HZF + Fe
c) HZF + Cu
d) untreated
cleaned
60s
90s
180s
300s
O_2
N_2 purged
i / Acm^{-2}
U / V_{SHE}
10^{-2}
10^{-3}
10^{-4}
10^{-5}
10^{-6}
10^{-7}
10^{-8}
-1,1
-1,0
-0,9
-0,8
-0,7
-0,6
-0,5
-0,4

DOI: 10.1016/j.electacta.2013.08.161
URN: urn:nbn:de:hbz:464-20201116-094204-8

This is the Authors Accepted Manuscript of an article published in: Electrochimica Acta 112 (2013) 14-23.
The final version may be found at: https://doi.org/10.1016/j.electacta.2013.08.161